Thin Solid Films 582 (2015) 176–179

Contents lists available at ScienceDirect

Thin Solid Films

journal homepage: www.elsevier.com/locate/tsf

Study of structural and optoelectronic properties of $Cu_2Zn(Sn_{1-x}Ge_x)Se_4$ (x = 0 to 1) alloy compounds

M. Grossberg *, K. Timmo, T. Raadik, E. Kärber, V. Mikli, J. Krustok

Department of Materials Science, Tallinn University of Technology, Ehitajate tee 5, 19086 Tallinn, Estonia

ARTICLE INFO

Available online 23 October 2014

Keywords:
$Cu_2Zn(Sn_{1-x}Ge_x)Se_4$
Kesterite
Photoluminescence
Raman scattering

ABSTRACT

In this work, the optoelectronic and structural properties of $Cu_2Zn(Sn_{1-x}Ge_x)Se_4$ (CZTGeSe) alloy compounds with x varying from 0 to 1 with a step of 0.1 were studied. The crystal structure and the lattice parameters of the CZTGeSe polycrystals were determined by using X-ray diffraction analysis. A linear decrease of the lattice parameter *a* from 0.569 nm to 0.561 nm with increasing Ge concentration was detected. Raman spectroscopy analysis revealed unimodal behavior and a linear shift of the three A symmetry Raman modes of kesterite crystal structure towards higher wavenumbers with increasing Ge content. Radiative recombination processes in CZTGeSe polycrystals were studied by using low-temperature photoluminescence (PL) spectroscopy. A continuous shift from 0.955 eV to 1.364 eV of the PL band position with increasing Ge concentration was detected. Based on the temperature dependent PL measurements of the CZTGeSe polycrystals, two types of recombination mechanisms were detected: band to impurity recombination in $Cu_2Zn(Sn_{1-x}Ge_x)Se_4$ with $x \leq 0.2$, and band to tail recombination in $Cu_2Zn(Sn_{1-x}Ge_x)Se_4$ with $x > 0.2$.

1. Introduction

The I_2–II–IV–VI_4 (I = Cu, Ag; II = Zn, Cd; IV = Si, Ge, Sn; VI = S, Se) series of quaternary chalcogenide semiconductors have drawn wide interest for their application as solar cell absorbers. $Cu_2ZnSn(S_xSe_{1-x})_4$ (CZTSSe) based solar cells have recently achieved solar energy conversion efficiency of 12.6% [1]. The bandgap energy of CZTSSe solid solutions can be tailored by varying the S/Se ratio to reach the optimum for solar energy conversion value of around 1.4 eV. In this study we show additional ability for tuning bandgap of CZTSe through substitution of Sn by Ge forming $Cu_2Zn(Sn_{1-x}Ge_x)Se_4$ (CZTGeSe) alloy compounds with x varying from 0 to 1. So far, Bag et al. [2] have reported the highest power conversion efficiency of 9.1% with CZTGeSe solar cells (40% of Sn was substituted by Ge).

Only few studies on the properties of $Cu_2ZnGeSe_4$ (CZGeSe) have been reported. It was recently shown by Morihama et al. [3] that based on the diffuse reflectance spectra of the $Cu_2Zn(Sn_{1-x}Ge_x)Se_4$ solid solution powders the room-temperature bandgap energy increases linearly from 0.99 eV (CZTSe) to 1.35 eV (CZGeSe). The reported experimental room-temperature bandgap energies for CZGeSe determined from optical absorption measurements [4–8], quantum efficiency (QE) curves [9], and spectroscopic ellipsometry data [10] vary in the range from 1.34 to 1.65 eV. The room-temperature bandgap energy of about 1.02 eV of CZTSe has been determined from QE [11] and optical absorption measurements [12]. The low-temperature bandgap energy of about 1.04 eV of CZTSe is estimated from the low-temperature photoluminescence (PL) measurements where exciton emission at 1.033 eV was detected [12]. Based on the available data, it should be possible to tune the bandgap energy of $Cu_2Zn(Sn_{1-x}Ge_x)Se_4$ in between 1.02 eV and about 1.5 eV by varying x from 0 to 1.

CZGeSe and CZTSe can crystallize in kesterite $I\bar{4}$ and stannite $I\bar{4}2m$ crystal structures, the kesterite being the ground state crystal structure [13,14]. However, due to the similarity of the two crystal structures that differ only by the ordering of isoelectronic Cu and Zn atoms in the cation sublattice, it is difficult to distinguish between the kesterite and stannite structure by conventional X-ray diffraction (XRD). By using neutron scattering analysis that can differentiate between the kesterite and stannite structure, Schorr et al. [15] have reported CZTSe to crystallize in the kesterite structure. It was recently shown by Morihama et al. [3] that $Cu_2Zn(Sn_{1-x}Ge_x)Se_4$ solid solution powders all crystallize in the kesterite crystal structure based on the Rietveld analysis of the XRD patterns. Moreover, it was also recently shown by Guc et al. [16] by using polarization dependent Raman scattering analysis that CZGeSe and CZTSe show vibrational spectra characteristic of the kesterite crystal structure.

The radiative recombination mechanisms in the kesterites like CZTS and CZTSe are still under debate and there are only few reports about the PL of CZTSe, CZGeSe and their solid solutions. In low-temperature PL measurements, broad asymmetric PL band at around 0.95 eV resulting from band-to-impurity (BI) recombination is usually detected in CZTSe [17–20], also excitonic emission at 1.033 eV together with donor–acceptor pair recombination at 0.989 eV involving shallow defects has been reported [12]. Bag et al. [2] have presented a broad PL spectrum

* Corresponding author.

http://dx.doi.org/10.1016/j.tsf.2014.10.055
0040-6090/

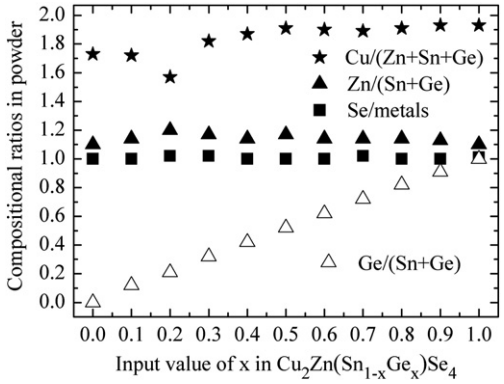

Fig. 1. Compositional ratios of the studied $Cu_2Zn(Sn_{1-x}Ge_x)Se_4$ powders with x from 0 to 1 with a step of 0.1, according to the EDS analysis.

of $Cu_2Zn(Sn_{1-x}Ge_x)Se_4$ with $x = 0.4$ at 1.05 eV. Timmo et al. [9] have reported a broad asymmetric PL spectrum of CZGeSe at 1.26 eV.

The results of the present study show the structural and vibrational properties together with the dominating recombination mechanisms of $Cu_2Zn(Sn_{1-x}Ge_x)Se_4$ polycrystals with x varying from 0 to 1 with a step of 0.1.

2. Experimental

$Cu_2Zn(Sn_{1-x}Ge_x)Se_4$ polycrystalline powders were synthesized from Cu, Zn, Sn, and Ge elemental metal powders and elemental Se in evacuated quartz ampoules. All precursors were grounded in an agate mortar in intended quantities and ratios. After mixing and grounding the precursors, the mixture was poured into a quartz ampoule, degassed under dynamic vacuum, sealed, and annealed isothermally at 1013 K for 168 h and at 823 K for 168 h. After annealing at 823 K, ampoules were cooled down with furnace to room temperature. In addition, post-growth heat treatment at 1013 K for 35 min was performed. After annealing the ampoules were cooled down with furnace to room temperature.

The chemical composition of the $Cu_2Zn(Sn_{1-x}Ge_x)Se_4$ polycrystals was determined by energy dispersive spectroscopy (EDS) on scanning electron microscope Zeiss ULTRA 55 operating at accelerating voltage of 20 kV and using Röntec EDX XFlash 3001 detector. Powder XRD patterns were recorded on a Rigaku Ultima IV diffractometer with Cu K_α radiation ($\lambda = 1.5406$ Å). Rietveld method was used for the derivation of crystal structure information from powder XRD data. The micro-Raman spectra were recorded by using a Horiba's LabRam HR800 spectrometer and 532 nm laser line that was focused on the sample with spot size of about 5 μm. For PL measurements, the samples were mounted in the closed-cycle He cryostat. The 405 nm laser line was used for PL excitation and InGaAs detector for signal detection.

3. XRD results

According to EDS analysis a linear substitution of Sn with Ge is observed in the CZTGeSe polycrystalline powders with initial composition of $Cu_{1.82}Zn_{1.18}Sn_{1-x}Ge_xSe_{4.02}$ with x from 0 to 1 with a step of 0.1, as presented in Fig. 1. Only for the CZTGeSe powder with $x = 0.2$ a deviation from the linear trend in composition was detected. The synthesized powders showed increase in the Cu content with increasing Ge content, probably due to the narrower single phase formation region of CZGeSe.

XRD patterns of $Cu_2Zn(Sn_{1-x}Ge_x)Se_4$ polycrystals in dependence of the x value were recorded. Lattice shrinkage with increasing substitution for the smaller Ge ion results in a systematic shift in the diffraction peaks to higher angles. From the diffraction patterns the lattice parameters were determined by using Rietveld refinements. The obtained values for CZTGeSe are in agreement with the data reported by Morihama et al. [3]. A linear trend in lattice parameters was observed (see Fig. 2a) indicating a homogeneous element distribution within each powder and the substitution of tin by germanium in $Cu_2Zn(Sn_{1-x}Ge_x)Se_4$. The tetragonal distortion parameter $\eta = c / 2a$ in dependence of the Ge content in the $Cu_2Zn(Sn_{1-x}Ge_x)Se_4$ powders is shown in Fig. 2b. For all the studied powders $\eta < 1$ that according to the theoretical predictions [21,22] is characteristic of the kesterite structure. Our findings are in very good agreement with the results reported by Morihama et al. [3].

4. Raman analysis results

The Raman spectra of $Cu_2Zn(Sn_{1-x}Ge_x)Se_4$ polycrystals are presented in Fig. 3. The Raman peaks of CZTSe are in agreement with previous reports [16,17,23,24] and can be detected at 81, 157, 168, 173, 196, 223, 234, and 245 cm^{-1}. The Raman peak positions of CZGeSe are also in agreement with previous reports by Timmo et al. [9] and Guc et al. [16] and were detected at 92, 174, 178, 205, 271, 283 and 292 cm^{-1}. Guc et al. [16] have performed detailed polarization dependent Raman analysis on CZGeSe and CZTSe crystals and assigned the detected Raman peaks to the corresponding symmetry modes characteristic of the kesterite type crystal structure. The irreducible representation for the zone center phonon modes for kesterite type structure with space group $I\bar{4}$ is [24]:

$$\Gamma = 3A + 6B + 6E,$$

where all modes are Raman active. The three A modes characteristic for the kesterite structure can be detected at 168, 173, and 196 cm^{-1} in the Raman spectrum of CZTSe polycrystalline powder and at 174, 178, and 205 cm^{-1} in the Raman spectrum of CZGeSe powder. Frequencies of all A modes corresponding to the vibrations of anion atoms shift linearly with x in $Cu_2Zn(Sn_{1-x}Ge_x)Se_4$ between the positions for CZTSe and CZTGeSe showing the expected unimodal behavior characteristic of alloy compounds where cations are substituted. Also, there was no

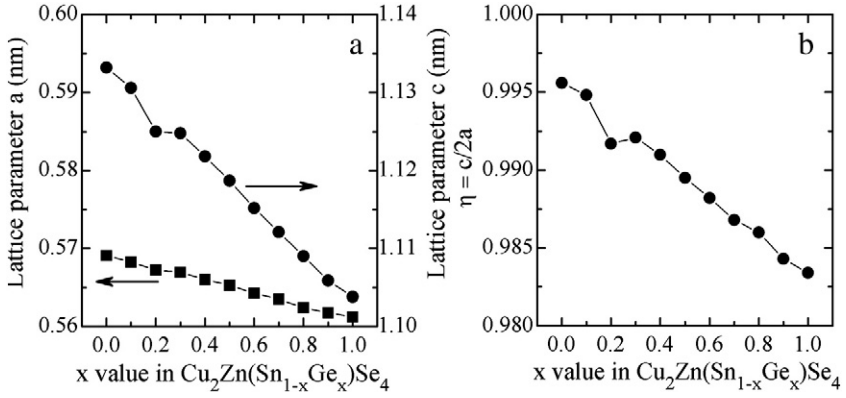

Fig. 2. a) Lattice parameters *a* and *c*, and b) tetragonal distortion parameter η in dependence of the Ge content in the $Cu_2Zn(Sn_{1-x}Ge_x)Se_4$ powders.

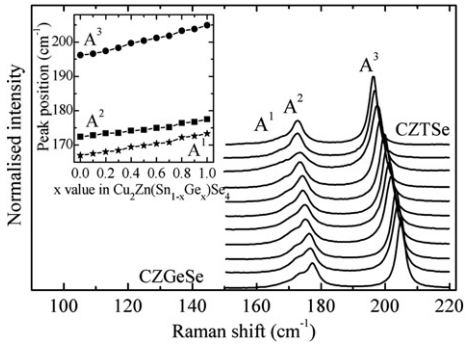

Fig. 3. Raman spectra of $Cu_2Zn(Sn_{1-x}Ge_x)Se_4$ polycrystals in dependence of the x value. The inset graph shows the linear shift of the peak positions of the three A symmetry modes towards higher wavenumbers with increasing Ge content.

significant broadening of the A modes with cation substitution. Accordingly, Raman results suggest kesterite crystal structure for the whole solid solution series of $Cu_2Zn(Sn_{1-x}Ge_x)Se_4$ polycrystals.

5. Photoluminescence results

Low-temperature ($T = 10$ K) PL spectra of $Cu_2Zn(Sn_{1-x}Ge_x)Se_4$ polycrystals in dependence of the x value are presented in Fig. 4. A continuous shift from 0.955 eV to 1.364 eV of broad and asymmetric PL band with increasing value of x from 0 to 1, is detected. The asymmetric shape of the PL band is characteristic to the semiconductor material with spatial potential fluctuations that are commonly present in the compensated multinary compounds with high native defect concentrations [17,25,26]. The PL spectra of studied $Cu_2Zn(Sn_{1-x}Ge_x)Se_4$ polycrystals show large blueshift in the order of about 15 meV/decade with increasing laser power that is also characteristic to a material with spatial potential fluctuations [25,26]. The PL band of CZTSe at 0.95 eV shows the same behavior and thermal activation energy of 70 meV as was also observed in our previous study [17]. Accordingly, it can be attributed to BI recombination involving an acceptor defect with ionization energy of 70 meV. The PL band shifts towards higher energies with increasing Ge concentration almost following the bandgap energy dependence on Ge content presented by Morihama et al. [3] (see the inset graph in Fig. 4).

To clarify the recombination mechanism, temperature dependencies of the PL spectra were measured and two types of behavior were detected. The thermal activation energies were determined from the Arrhenius plot where the linear (in the case of BI recombination) or nearly linear (in the case of band-to-tail (BT) recombination) dependence of

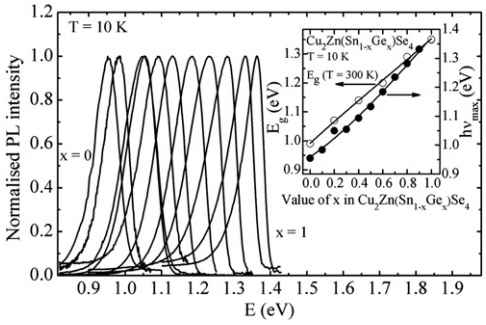

Fig. 4. Low-temperature PL spectra of $Cu_2Zn(Sn_{1-x}Ge_x)Se_4$ polycrystals with varying values of x. The PL peaks relate to 0.1 increments in x from left to right. The inset graph shows shift of the detected PL band peak position (solid dots) that is slightly steeper than the bandgap energy dependence (hollow dots) on Ge content as presented by Morihama et al. [3] indicating change in the recombination mechanism. Note that room temperature bandgap energy values with 0.2 increments in x were given in [3]. Solid lines present polynomial fits of the dependencies.

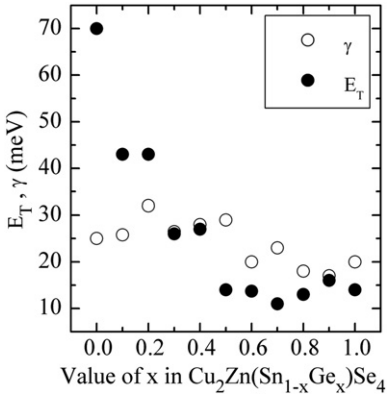

Fig. 5. Thermal activation energies E_T (solid dots) obtained from the temperature dependencies of the PL spectra of $Cu_2Zn(Sn_{1-x}Ge_x)Se_4$ polycrystals. The average depth of the spatial potential fluctuations γ in $Cu_2Zn(Sn_{1-x}Ge_x)Se_4$ is presented with hollow dots.

$\ln I(T)$ versus $1000/T$ at high temperatures was fitted by using theoretical expression for discrete energy levels [27]:

$$\Phi(T) = \frac{\Phi_0}{1 + \alpha_1 T^{3/2} + \alpha_2 T^{3/2} \exp\left(-E_T/kT\right)}, \quad (1)$$

where Φ is integrated intensity, α_1 and α_2 are the process rate parameters and E_T is the thermal activation energy. The obtained thermal activation energies E_T (see Fig. 5) for $Cu_2Zn(Sn_{1-x}Ge_x)Se_4$ polycrystals with $x \leq 0.2$ are in the range from 43 to 70 meV. Thermal activation energies in the range from 11 to 27 meV were obtained for $Cu_2Zn(Sn_{1-x}Ge_x)Se_4$ powders with $x > 0.2$. It was also observed that for $Cu_2Zn(Sn_{1-x}Ge_x)Se_4$ with $x > 0.2$, the PL band becomes more asymmetric with more pronounced exponential low-energy side that is characteristic for BT recombination. BT band results from recombination of free electrons and holes localized in the valence band tail caused by the spatial potential fluctuations. The potential fluctuations lead to local perturbation of the band structure, thus broadening the defect level distribution and forming band tails. The density of the band tail states usually has an exponential shape resulting in an exponential tail of the low-energy side of the PL band. The BI recombination involves deeper acceptor defects that do not overlap with the valence band tail. The average depth of the spatial potential fluctuations γ can be determined from the shape of the low-energy side of the PL band (see details in Refs. [25,26]) and was found to vary in between 17 and 32 meV in studied CZTGeSe (see Fig. 5). Accordingly, one could conclude that in the studied CZTGeSe polycrystals with $x \leq 0.2$ BI recombination dominates since the depth of the fluctuations is smaller than the obtained thermal activation energies resembling the ionization energies of the corresponding acceptor defects. In CZTGeSe polycrystals with $x > 0.2$, the BT recombination dominates. In case of BT recombination, the obtained thermal activation energies enable us to estimate the ionization energy of the pseudo-acceptor defects in the valence band tail that is in the range from 11 to 27 meV. The observed change in the recombination mechanism can also be seen in the steeper dependence of the PL band peak position on the Ge content in comparison to the bandgap energy (see inset graph in Fig. 4).

6. Conclusion

$Cu_2Zn(Sn_{1-x}Ge_x)Se_4$ polycrystalline powders with x varying from 0 to 1 were studied by XRD, Raman scattering and PL spectroscopy. The kesterite crystal structure of CZTGeSe was determined from the XRD and Raman analyses. Based on the temperature dependent PL measurements of the CZTGeSe polycrystals, two types of recombination mechanisms were detected: BI recombination in

$Cu_2Zn(Sn_{1-x}Ge_x)Se_4$ with $x \leq 0.2$, and BT recombination in $Cu_2Zn(Sn_{1-x}Ge_x)Se_4$ with $x > 0.2$.

Acknowledgments

This work was supported by the Estonian Science Foundation grants ETF9369 and ETF9425, by the institutional research funding IUT 19-28 of the Estonian Ministry of Education and Research, the Estonian Centre of Excellence in Research, Project TK117, and by the Estonian Material Technology Programme, Project AR12128.

References

[1] Wei Wang, Mark T. Winkler, Oki Gunawan, Tayfun Gokmen, Teodor K. Todorov, Yu Zhu, David B. Mitzi, Device characteristics of CZTSSe thin-film solar cells with 12.6% efficiency, Advanced Energy Materials, DOI: 10.1002/aenm.201301465.
[2] Santanu Bag, Oki Gunawan, Tayfun Gokmen, Yu Zhu, David B. Mitzi, Hydrazine-processed Ge-substituted CZTSe solar cells, Chem. Mater. 24 (2012) 4588.
[3] Masaru Morihama, Feng Gao, Tsuyoshi Maeda, Takahiro Wada, Crystallographic and optical properties of $Cu_2Zn(Sn_{1-x}Ge_x)Se_4$ solid solution, Jpn. J. Appl. Phys. 53 (2014) 04ER09-1.
[4] Chong-Il Lee, Chang-Dae Kim, Optical properties of undoped and Co^{2+}-doped $Cu_2ZnGeSe_4$ crystals, J. Korean Phys. Soc. 37 (2000) 364.
[5] Christophe P. Heinrich, Tristan W. Day, Wolfgang G. Zeier, G. Jeffrey Snyder, Wolfgang Tremel, Effect of isovalent substitution on the thermoelectric properties of the $Cu_2ZnGeSe_{4-x}S_x$ series of solid solutions, J. Am. Chem. Soc. 136 (2014) 442.
[6] H. Matsushita, T. Maeda, A. Katsui, T. Takizawa, Thermal analysis and synthesis from the melts of Cu-based quaternary compounds Cu–III–IV–VI_4 and Cu_2–II–IV–VI_4 (II = Zn, Cd; III = Ga, In; IV = Ge, Sn; VI = Se), J. Cryst. Growth 208 (2000) 416.
[7] H. Matsushita, T. Ochiai, A. Katsui, Preparation and characterization of $Cu_2ZnGeSe_4$ thin films by selenization method using the Cu–Zn–Ge evaporated layer precursors, J. Cryst. Growth 275 (2005) e995.
[8] P. Uday Bhaskar, G. Suresh Babu, Y.B. Kishore Kumar, V. Sundara Raja, Preparation and characterization of co-evaporated $Cu_2ZnGeSe_4$ thin films, Thin Solid Films 534 (2013) 249.
[9] K. Timmo, M. Kauk-Kuusik, M. Altosaar, J. Raudoja, T. Raadik, M. Grossberg, T. Varema, M. Pilvet, I. Leinemann, O. Volobujeva, E. Mellikov, Novel Cu_2CdSnS_4 and $Cu_2ZnGeSe_4$ absorber materials for monograin layer solar cell application, Proceedings of the 28th European Photovoltaic Solar Energy Conference, Paris, France, Sept 30–Oct 4, 2013, EU PVSEC Proceedings, 2013, p. 2385.
[10] M. Leon, S. Levcenko, R. Serna, A. Nateprov, G. Gurieva, J.M. Merino, S. Schorr, E. Arushanov, Spectroscopic ellipsometry study of $Cu_2ZnGeSe_4$ and $Cu_2ZnSiSe_4$ polycrystals, Mater. Chem. Phys. 141 (2013) 58.
[11] J. Krustok, R. Josepson, T. Raadik, M. Danilson, Potential fluctuations in $Cu_2ZnSnSe_4$ solar cells studied by temperature dependence of quantum efficiency curves, Physica B 405 (2010) 3186.
[12] F. Luckert, D.I. Hamilton, M.V. Yakushev, N.S. Beattie, G. Zoppi, M. Moynihan, I. Forbes, A.V. Karotki, A.V. Mudryi, M. Grossberg, J. Krustok, R.W. Martin, Optical properties of high quality $Cu_2ZnSnSe_4$ thin films, Appl. Phys. Lett. 99 (2011) 062104.
[13] Shiyou Chen, Aron Walsh, Ye Luo, Ji-Hui Yang, X.G. Gong, Su-Huai Wei, Wurtzite-derived polytypes of kesterite and stannite quaternary chalcogenide semiconductors, Phys. Rev. B 82 (2010) 195203.
[14] J. Paier, R. Asahi, A. Nagoya, G. Kresse, Cu_2ZnSnS_4 as a potential photovoltaic material: a hybrid Hartree–Fock density functional theory study, Phys. Rev. B 79 (2009) 115126.
[15] S. Schorr, H.J. Hoebler, M. Tovar, A neutron diffraction study of the stannite–kesterite solid solution series, Eur. J. Mineral. 19 (2007) 65.
[16] M. Guc, S. Levcenko, V. Izquierdo-Roca, X. Fontane, E. Arushanov, A. Perez-Rodriguez, Polarized Raman scattering analysis of $Cu_2ZnSnSe_4$ and $Cu_2ZnSnGeSe_4$ single crystals, J. Appl. Phys. 114 (2013) 193514.
[17] M. Grossberg, J. Krustok, K. Timmo, M. Altosaar, Radiative recombination in $Cu_2ZnSnSe_4$ monograins studied by photoluminescence spectroscopy, Thin Solid Films 517 (2009) 2489.
[18] Alex Redinger, Katja Hönes, Xavier Fontané, Victor Izquierdo-Roca, Edgardo Saucedo, Nathalie Valle, Alejandro Pérez-Rodríguez, Susanne Siebentritt, Detection of a ZnSe secondary phase in coevaporated $Cu_2ZnSnSe_4$ thin films, Appl. Phys. Lett. 98 (2011) 101907.
[19] O. Zaberca, F. Oftinger, J.Y. Chane-Ching, L. Datas, A. Lafond, P. Puech, A. Balocchi, D. Lagarde, X. Marie, Surfactant-free CZTS nanoparticles as building blocks for low-cost solar cell absorbers, Nanotechnology 23 (2012) 185402.
[20] P.M.P. Salomé, P.A. Fernandes, A.F. da Cunha, J.P. Leitão, J. Malaquias, A. Weber, J.C. González, M.I.N. da Silva, Growth pressure dependence of $Cu_2ZnSnSe_4$ properties, Sol. Energy Mater. Sol. Cells 94 (2010) 2176.
[21] X.G. Shiyou Chen, A. Walsh Gong, S.H. Wei, Crystal and electronic band structure of Cu_2ZnSnX_4 (X = S and Se) photovoltaic absorbers: first-principles insights, Appl. Phys. Lett. 94 (2009) 041903.
[22] Heng-Rui Liu, Shiyou Chen, Ying-Teng Zhai, H.J. Xiang, X.G. Gong, Su-Huai Wei, First-principles study on the effective masses of zinc-blend-derived Cu_2Zn–IV–VI_4 (IV = Sn, Ge, Si and VI = S, Se), J. Appl. Phys. 112 (2012) 093717.
[23] Rabie Djemour, Alex Redinger, Marina Mousel, Levent Gütay, Xavier Fontane, Victor Izquierdo-Roca, Alejandro Perez-Rodriguez, Susanne Siebentritt, The three A symmetry Raman modes of kesterite in $Cu_2ZnSnSe_4$, Opt. Express 21 (2013) A695.
[24] T. Gürel, C. Sevik, T. Cagin, Characterization of vibrational and mechanical properties of quaternary compounds Cu_2ZnSnS_4 and $Cu_2ZnSnSe_4$ in kesterite and stannite structures, Phys. Rev. B 84 (2011) 205201.
[25] A.P. Levanyuk, V.V. Osipov, Edge luminescence of direct-gap semiconductors, Sov. Phys. Usp. 24 (1981) 187.
[26] J. Krustok, H. Collan, M. Yakushev, K. Hjelt, The role of spatial potential fluctuations in the shape of the PL bands of multinary semiconductor compounds, Phys. Scr. T79 (1999) 179.
[27] J. Krustok, H. Collan, K. Hjelt, Does the low temperature Arrhenius plot of the photoluminescence intensity in CdTe point towards an erroneous activation energy? J. Appl. Phys. 81 (1997) 1442.